

Equivalent circuit model modified for free-standing bilayer lipid membranes beyond $1\text{ T}\Omega$

Yasutaka Tomioka^{1*}, Shogo Takashima¹, Masataka Moriya¹, Hiroshi Shimada¹, Fumihiko Hirose², Ayumi Hirano-Iwata³ and Yoshinao Mizugaki¹

¹*The University of Electro-Communications, Chofu, Tokyo, 182-8585, Japan.*

²*Yamagata University, Yonezawa, Yamagata, 992-8510, Japan*

³*Tohoku University, Aoba, Sendai, 980-8577, Japan*

*E-mail: tomioka@w8-7f.ee.uec.ac.jp

A cell is the basic functional unit of living organisms. Bilayer lipid membranes (BLMs), which form cell membranes can be assembled by using artificial methods. The electrochemical characteristics of BLMs are normally investigated using electrochemical impedance spectroscopy (EIS); however, the equivalent circuit need to be modified by the experimental conditions. In this study, we formed plain BLMs to determine the underlying equivalent circuit model of free-standing BLMs, and we measured the electrical characteristics using EIS. To analyze the results of EIS, we proposed equivalent circuit models including electrical double layer effects on both sides of a BLM. We also extracted and evaluated the electrochemical parameters; the aperture-suspended BLMs using an Si chip having tapered edge recorded $\text{T}\Omega$ -order membrane resistances, which were one order higher than those reported in most previous studies. Regarding the capacitances of electrical double layers (EDLs), we compared the extracted values and the calculated results.

1. Introduction

A cell is the basic functional unit of living organisms. The cell membrane separates the interior from the exterior, and regulates the transport of many substances. A bilayer lipid membrane (BLM), which is mainly composed of a cell membrane, can be formed using artificial methods for embedding ion-channel proteins. For example, free-standing BLMs using the folding method¹⁾ or the painting method²⁾ are assembled in the form of aperture-suspended BLMs. The mechanical stability or the life time of free-standing BLMs, which formed these methods depends on a micro- and nano-structures^{3,4)} of a suspending chip and the aperture size.⁵⁾ In other cases, supported lipid membranes⁶⁾ (SLMs) and tethered bilayer lipid membranes^{7,8)} (t-BLMs) are devised. BLMs formed by using these methods have high stability;⁹⁻¹⁰⁾ however, they also have some problems. For instance, close surface proximity may denature the protein embedded in BLMs.¹¹⁾ In addition, these BLMs tend to record low membrane resistances.¹²⁾ Both problems disturb the monitoring single channel events. To overcome these problems, advanced Si chips were fabricated.^{3,4,13-15)} The Si chip has a sufficiently large aperture to fuse the proteins, and has a tapered edge to enhance durability; BLMs suspended from the aperture of the Si chip recorded long lifetimes.⁴⁾

To measure the electrochemical characteristics of BLMs, electrochemical impedance spectroscopy (EIS) is commonly conducted. This method is commonly used for many electrochemical measurements, biosensors,¹⁶⁾ and so on. The electrical characteristics of BLMs can be extracted and evaluated using equivalent circuit fittings. Membrane resistances and capacitances are typically measured by EIS; therefore, it is important to design suitable circuit models.^{17,18)} An ordinary biological membrane is simply expressed as a resistor-capacitor parallel circuit; however, this traditional model is not suitable for artificially formed BLMs because the overall impedance is affected by other elements, such as the supporting chip or the substrate, the surface charge of the hydrophilic heads of lipid bilayers and the condition of the solution. In particular, the electrical double layer (EDL) formed by the surface charge of BLM influences the electrical characteristics.^{5,14)}

In this study, we formed plain free-standing BLMs by using a folding method, and we investigated the fundamental electrochemical characteristics of the BLMs by measuring their AC characteristics using EIS. In addition, we proposed equivalent circuit models, which included electrochemical parameters that reproduced EDL effects on both sides of the BLM. A suitable model was selected by plots of fitting error. Moreover, we extracted electrochemical parameters from the proposed equivalent circuit model and evaluated the circuit parameters of a BLM, an Si chip, and EDLs; we obtained $T\Omega$ -order membrane

resistances.

2. Experimental methods

Figure 1 shows the schematic drawing of the overall experimental setup and procedure. Figure 1(a) shows a schematic illustration of the Teflon chambers and the measurement system. A mixed solution containing 2 M KCl, 5 mM HEPES and KOH was used as a buffer. Ag/AgCl electrodes were processed by electrolysis in 0.2 M KCl solution. Figure 1(b) shows the schematic illustrations of a detailed design of the Si chip and aperture-suspended BLM. Si chips were processed as described in Refs 3 and 4. Figure 1(c) shows a BLM-forming procedure (the folding method).¹⁾ Buffer solution (1,400 μ L) was poured into both sides of the wells and the solution level decreased using the attached syringes. Then, 5 mg/mL 1,2-diphytanoyl-sn-glycero-3-phosphocholine (DPhPC), which is a mixed solution of 10 mg/mL DPhPC-chloroform and hexane, was dropped into both sides of the wells. After vaporizing chloroform and hexane, a BLM was formed at the aperture of the Si chip by raising the buffer solution level. The AC characteristics of BLMs were measured in a Faraday cage on an anti-vibration table. EIS was conducted with a potentiostat (Bio-Logic, SP-300) in the frequency range from 1 MHz to 1 mHz with the signal amplitude of 70 mV. Equivalent circuit fitting was operated by using software (ZView®, Scribner Associates Inc.), excluding the initial and last two plots.

3. Equivalent circuit model for a free-standing bilayer lipid membrane

3.1 Establishment of equivalent circuit models

Figure 2(a) shows the equivalent circuit model I proposed in a previous study.¹⁷⁾ The parallel R_{BLM} and C_{BLM} correspond to the BLM resistance and capacitance, which are in parallel with the C_{CHIP} of the Si chip's capacitance, and R_{E} is the overall series resistance. Equivalent circuit I is a unique model because it includes the effect of EDL formed on the BLM surface; the parallel R_{EDL} and Q_{EDL} correspond to the charge-transfer resistance and EDL capacitance. Q_{EDL} is known as the constant phase element (CPE),^{5,17-20)} which reproduces the electrostatic capacity of the EDL on the BLM surface; the CPE is generally used for electrochemical analysis. Based on the previous study,¹⁷⁾ we proposed equivalent circuit models II and III including the effects of EDLs on both sides of a BLM as shown in Fig. 2(b). In the equivalent circuit model II and III, the capacitances and the CPEs,

respectively, are used as the components for EDL. Moreover, both circuit models II and III includes the parallel R_M and C_M , which are the effect of the measuring equipment to reproduce the one peak of the phase curve appearing every measurement.

3.2 Parameters for the equivalent circuit

The measured results of EIS were extracted by equivalent circuit fitting. We constructed equivalent circuit models with typical electrical parameters and electrochemical parameters. At first, the overall series resistance is shown as R_E , which includes access resistance.²¹⁾ The access resistance at the aperture of the Si chip is written as

$$R_{\text{ac-aperture}} = \frac{1}{2\kappa d}. \quad (1)$$

Here, κ is the conductivity of the buffer solution, and d is the diameter of the Si chip aperture. Access resistance exists at both sides of the aperture;²²⁾ therefore, the total access resistance at the aperture becomes double. In addition, as shown in Fig. 1(b), it is necessary to estimate the resistance of the square frustum area (upper base $a = 100 \mu\text{m}$, lower base $b = 400 \mu\text{m}$). As a function of height l , the area $S(l)$ at the height l is expressed as

$$S(l) = \frac{b^2 - a^2}{L_{\text{Si}}} l + a^2. \quad (2)$$

Here, L_{Si} is the height of the square frustum (equal to the thickness of Si). Therefore, the resistance of the square frustum area is calculated as follows:

$$R_{\text{frustum}} = \frac{1}{\kappa} \int_0^{L_{\text{Si}}} \frac{1}{S(l)} dl = \frac{1}{\kappa} \int_0^{L_{\text{Si}}} \frac{1}{\frac{b^2 - a^2}{L_{\text{Si}}} l + a^2} dl = \frac{2L_{\text{Si}}}{\kappa(b^2 - a^2)} \ln \frac{b}{a}. \quad (3)$$

The access resistance at the lower base of the frustum $R_{\text{ac-frustum}}$ is expressed as

$$R_{\text{ac-frustum}} = \frac{1}{2\kappa b}. \quad (4)$$

Generally, the access resistance is determined for a circular aperture;²¹⁾ we approximated $R_{\text{ac-frustum}}$ for a circular aperture $400 \mu\text{m}$ in diameter. By using Eqs. (1), (3), and (4), we can express the overall theoretical resistance of R_E as follows:

$$R_E = 2R_{\text{ac-aperture}} + R_{\text{frustum}} + R_{\text{ac-frustum}}. \quad (5)$$

An equally important parameter is the CPE,^{5,17-20)} which reproduces the impedance of EDL with the parallel R_{EDL} element. The electrochemical impedance of CPE is written as follows:

$$Z_{\text{CPE}} = \frac{1}{(j\omega)^\alpha Q}. \quad (6)$$

Q and α used in Eq. (6) are important parameters. Here, Z_{CPE} behaves as a pure capacitance in the case of $\alpha = 1$. On the other hand, Z_{CPE} behaves as a pure resistance when $\alpha = 0$. The unit of Q is generally expressed as $\text{Fs}^{\alpha-1}$, where F is Farad (the unit of

electrostatic capacity), and s is second (the unit of time). If it is assumed that Z_{EDL} is a parallel component of the resistance R_{EDL} and Z_{CPE} , the real and imaginary parts of Z_{EDL} can be expressed as

$$\begin{cases} \text{Re}(Z_{EDL}) = \frac{R_{EDL}(1+\omega^\alpha R_{EDL}Q \cos\frac{\alpha\pi}{2})}{(1+\omega^\alpha R_{EDL}Q \cos\frac{\alpha\pi}{2})^2 + (\omega^\alpha R_{EDL}Q \sin\frac{\alpha\pi}{2})^2} \\ \text{Im}(Z_{EDL}) = \frac{\omega^\alpha R_{EDL}^2 Q \sin\frac{\alpha\pi}{2}}{(1+\omega^\alpha R_{EDL}Q \cos\frac{\alpha\pi}{2})^2 + (\omega^\alpha R_{EDL}Q \sin\frac{\alpha\pi}{2})^2} \end{cases} \quad (7)$$

Equation (7) includes the electrochemical parameters of Q ; therefore, it is necessary that the parameters of Q are converted for effective ELD capacitance C_{EDL} .²⁰⁾ The effective capacitance associated with the CPE is expressed as follows:

$$C_{EDL} = Q^{1/\alpha} R_{EDL}^{(1-\alpha)/\alpha}. \quad (8)$$

4. Results and discussion

4.1 Equivalent circuit fitting and evaluation

Figure 3(a) shows the plots obtained by EIS measurement and the fitting curves of the circuit models I, II, and III. At very low frequencies (1 -10 mHz), the impedance spectrum reaches $T\Omega$ order, and the phase spectrum rises monotonously. This indicates that the BLM behaves resistively; and it shows $T\Omega$ -order membrane resistance. Moreover, the phase spectrum has three peaks; it means that the equivalent circuit model has three or more resistance-capacitance or resistance-CPE parallel components apart from the R_{BLM} - C_{BLM} parallel component. EIS was conducted three times, and each result showed similar behavior ($|Z|$ at 1 Hz: 3.45, 3.54, and 2.04 $G\Omega$; θ at 1 Hz: -83.2° , -82.3° , and -81.0° ; $|Z|$ at 1 MHz: 14.5, 17.9, and 18.2 $k\Omega$; θ at 1 MHz: -63.1° , -62.2° , and -60.9°). Figure 3(b) shows the fitting errors between the plots obtained by the EIS measurement and the fitting curves. As shown in Fig. 3(b), the fitting errors of circuits I and II tended to be higher than that of circuit model III in the high-frequency region (1 kHz -1 MHz). In conclusion, the EDL components (parallel R_{EDL} and Q_{EDL}) improve the fitting accuracy; circuit model III is the most suitable model among these three circuit models.

4.2 Discussion of the extracted parameters

Table I shows the fitting parameters extracted from the equivalent circuit models I, II, and III. As shown in Tab. I, the membrane resistance R_{BLM} of 2.34 $T\Omega$ was obtained, which is one order higher than that obtained in many previous researches.^{5,8-12,17,18,23-28)} One reason for $T\Omega$ -order resistance could be that the micro- and nano-structures of the Si chip enhanced the durability of a BLM and prevented ion leakage through the lipid bilayer. Moreover, to

measure such a high membrane resistance, we introduced sensitive equipment of SP-300 as a chemical potentiostat that could detect very low currents, which enabled the TΩ-order resistance observation. There are many studies about the on-chip type BLMs (SLM and t-BLM); although these types of BLMs have some merits, the aperture-suspended-type BLM (free-standing BLM) is superior in terms of insulation.

On the other hand, the total value of the capacitance of the membrane C_{BLM} and the capacitance of the Si chip C_{CHIP} was 59.4 pF. To estimate C_{BLM} , we calculated the area of the aperture. The diameter of the aperture of the Si chip used in this work was approximately 51 μm, and the area was approximately 2043 μm². Using 0.4-0.9 μF/cm² as the specific capacitance of a BLM,^{4,24)} C_{BLM} was obtained as 8.24-18.5 pF. By subtracting this value from the total capacitance of 59.4 pF, C_{CHIP} was estimated to be in the range of 40.5-50.8 pF.

The series resistance R_E can be estimated from Eq. (5). $R_E = 5.32$ kΩ obtained from the circuit model III was approximately six times higher than the calculated results of 0.81 kΩ ($2R_{\text{ac-aperture}} = 0.65$ kΩ, $R_{\text{frustum}} = 0.12$ kΩ, $R_{\text{ac-frustum}} = 0.04$ kΩ). Therefore, the impedance of the electrodes needed to be considered in eq. (5). As shown in Fig. 3(b), errors tend to be large, especially in the very-low-frequency region (1 mHz -10 mHz) and in the high-frequency region (1 kHz -1 MHz). For the problem of the equivalent circuit model III, it is necessary to consider the impedance of the Ag/AgCl electrodes with the Warburg element or other suitable components. Low-frequency measurements are challenging because they need long measurement time and extremely small current detection. Moreover, BLM affected by time changes; therefore, it is difficult to reduce the errors at low frequencies.

It is necessary to discuss the parameters of EDLs. There are three typical theories describing double layer capacitances: Helmholtz, Gouy-Chapman and Stern's theory. The Helmholtz model assumes a parallel-plate capacitor, whereas the Gouy-Chapman model assumes Boltzmann distribution. The Stern model is a synthesis of both models. Based on Gouy-Chapman's theory,²⁹⁻³⁰⁾ the potential distribution and the EDL capacitance are obtained from the Poisson equation solving. The theoretical EDL capacitance is written as

$$C_{\text{GC}} = \sqrt{\frac{2\varepsilon\varepsilon_0 n_0 e^2}{kT}} \cosh\left(\frac{e\varphi_0}{kT}\right). \quad (9)$$

Here, n_0 is bulk concentration of the KCl buffer solution, and φ_0 is the surface potential; φ_0 obtained from Poisson equation is written as

$$\varphi_0 = \frac{2kT}{e} \sinh^{-1}\left(\frac{\sigma}{\sqrt{8\varepsilon\varepsilon_0 n_0 kT}}\right). \quad (10)$$

Here, σ is the surface charge density, which is determined by the occupied area of the

DPhPC head group, which is 77 \AA^2 .³¹⁾ Against Gouy-Chapman theory, we calculated the EDL capacitance using Kornyshev's theory.³²⁾ This theory has mean-field character based on the Poisson-Boltzmann lattice-gas model and was modified to account for the finite volumes occupied by the ions. Kornyshev's EDL capacitance is written as follows:

$$C_{GC} = \frac{\varepsilon\varepsilon_0}{4\pi L_D} \frac{\cosh\left(\frac{u_0}{2}\right)}{1+2\gamma\sinh^2\left(\frac{u_0}{2}\right)} \sqrt{\frac{2\gamma\sinh^2\left(\frac{u_0}{2}\right)}{\ln\left\{1+2\gamma\sinh^2\left(\frac{u_0}{2}\right)\right\}}}. \quad (11)$$

Here γ is equal to $2n_0/n_{\max}$, the dimensionless potential of u_0 is equal to $e\varphi_0/kT$, and the Debye length of L_D is equal to $\sqrt{\varepsilon\varepsilon_0 kT/2\pi e^2 n_0}$. Figure 4(a) shows the theoretical curves of EDL capacitances calculated by Gouy-Chapman's and Kornyshev's theory. EDL capacitance of Gouy-chapman's theory is clearly higher than the extracted results of 53.6 pF and 127 pF. Figure 4(b) shows the details of Kornyshev's theoretical capacitance curve for several ion concentration, which exhibits good agreement with the extracted values in condition of the dielectric constant range from 2.09 to 8.36. For most of ionic liquids, the value of epsilon varies near 10;³³⁾ therefore, calculated EDL capacitances are reliable.

5. Conclusions

We formed plain free-standing BLMs using a folding method, and we investigated the electrochemical characteristics of BLMs. The proposed equivalent circuit models II and III based on previous research¹⁷⁾ include EDL effects on both sides of a BLM. We found that the fitting errors of the circuit model III that adopt CPEs was lower than the circuit model II adopting capacitances. We also evaluated the electrochemical parameters extracted from the fitting results of the circuit model III, and found that the obtained membrane resistance of 2.34 TΩ is higher than many previous researches reporting GΩ-order resistance;^{5,8-12,17,18,23-28)} the tapered edge of the Si chip increased the membrane resistance. Regarding the capacitances of EDLs, we compared the extracted values and the calculated results. The theoretical curves expected from Gouy-Chapman's theory²⁹⁻³⁰⁾ was much higher than the extracted values, whereas the calculated results of Kornyshev's theory³²⁾ showed good conformity with the obtained parameters by assuming dielectric constants of 2.09 and 8.36.

Acknowledgments

This work was partly supported by JST-CREST Grant Number JPMJCR14F, and by JSPS KAKENHI Grant Number 17K04979. Nation-wide Cooperative Research Projects, Research Institute of Electrical Communication, Tohoku University are also acknowledged.

References

- 1) M. Montal and P. Mueller, PNAS **69**, 3561 (1972).
- 2) R. Benz, O. Frohlich, P. Lauger, M. Montal, Biochim. Biophys. Acta **394**, 323 (1975).
- 3) D. Tadaki, D. Yamaura, S. Araki, M. Yoshida, K. Arata, T. Ohori, K. Ishibashi, M. Kato, T. Ma, R. Miyata, Y. Tozawa, H. Yamamoto, M. Niwano and A. Hirano-Iwata, Sci. Rep. **7**, 17736 (2017).
- 4) D. Tadaki, D. Yamaura, K. Arata, T. Ohori, T. Ma, H. Yamamoto, M. Niwano and A. Hirano-Iwata, Jpn. J. Appl. Phys. **57**, 03EA01 (2018).
- 5) M. S. Khan, N. S. Dosoky, B. K. Berdiev and J. D. Williams, Eur. Biophys. J. **45**, 843 (2016).
- 6) L. K. Tamm and H. M. McConnell, Biophys. J. **47**, 105 (1985).
- 7) B. Raguse, V. Braachmaksvytis, B. A. Cornell, L. G. King, P. D. J. Osman, R. J. Pace and L. Wiczorek, Langmuir **14**, 648 (1998).
- 8) J. Andersson, J. J. Knobloch, M. V. Perkins, S. A. Holt and I. Köper, Langmuir **33**, 4444 (2017).
- 9) K. Sugihara, J. Voros and T. Zambelli, J. Am. Chem. Soc. **4**, 5047 (2010).
- 10) M. Andersson, H. M. Keizer, C. Zhu, D. Fine, A. Dodabalapur and R. S. Duran, Langmuir **23**, 2924 (2007).
- 11) M. S. Khan, N S. Dosoky, G. Mustafa, D. Patel, B. Berdiev and D. Williams, Langmuir **33**, 13680 (2017).
- 12) X. Wang, Y. Zhang, H. Bi and X. Han, RSC Adv. **6**, 72821 (2016).
- 13) A. Hirano-Iwata, K. Aoto, A. Oshima, T. Taira, R. Yamaguchi, Y. Kimura and M. Niwano, Langmuir **26**, 1949 (2010).
- 14) A. Oshima, A. Hirano-Iwata, H. Mozumi, Y. Ishinari, Y. Kimura and M. Niwano, Anal. Chem. **85**, 4363 (2013).
- 15) D. Yamaura, D. Tadaki, S. Araki, M. Yoshida, K. Arata, T. Ohori, K. Ishibashi, M. Kato, T. Ma, R. Miyata, H. Yamamoto, R. Tero, M. Sakuraba, T. Ogino, M. Niwano and A. Hirano-iwata, Langmuir **34**, 5615 (2018).
- 16) M. Aydin, E. B. Aydin and M K. Sezginturk, Biosens. Bioelectron. **107**, 1 (2018).
- 17) Z.-W. Zhu, Y. Wang, X. Zhang, C.-F. Sun, M.-G. Li, J.-W. Yan and B.-W. Mao, Langmuir **28**, 14739 (2012).
- 18) M. Zhang, Q. Zhai, L. Wan, L. Chen, Y. Peng, C. Deng, J. Xiang and J. Yan, Anal. Chem. **90**, 7422 (2018).
- 19) B. Hirschorn, M. E. Orazem, B. Tribollet, V. Vivier, I. Frateur and M. Musiani,

- Electrochim. Acta **55**, 6218 (2010).
- 20) B. Hirschorn, M. E. Orazem, B. Tribollet, V. Vivier, I. Frateur and M. Musiani, J. Electrochem. Soc. **157**, C452 (2010).
- 21) J. E. Hall, J. Gen. Physiol. **66**, 531 (1975).
- 22) I. Vodyanoy and S. M. Bezrukov, Biophys. J. **62**, 10 (1992).
- 23) T. Kaufeld, C. Steinem and C. F. Schmidt, J. Phys. D **48**, 025401 (2015).
- 24) C. G. Cranfield, S. T. Henriques, B. Martinac, P. Duckworth, D. J. Craik and B. Cornell, Langmuir **33**, 6630 (2017).
- 25) W. Romer and C. Steinem, Biophys. J. **86**, 955 (2004).
- 26) S. Rameshkumar and M. Kumaravel, Electrochim. Acta **245**, 489 (2017).
- 27) M. Alagappan, A. Kandaswamy, M. Kumaravel and S. Rameshkumar, Arab. J. Chem. (2017).
- 28) X. Han, A. Studer, H. Sehr, I. Geissbühler, M. D. Berardino, F. K. Winkler and L. X. Tiefenauer, Adv. Mater. **19**, 4466 (2007).
- 29) G. Gouy, J. Phys. Radium **9**, 457 (1910).
- 30) D. L. Chapman, Philos. Mag. **25**, 457 (1913).
- 31) K. Shinoda, W. Shinoda, T. Baba and M. Mikami, AIP **121**, 9648 (2004).
- 32) A. A. Kornyshev, J. Phys. Chem. B. **111**, 5545 (2007).
- 33) M. V. Fedorov and A. A. Kornyshev, Electrochim. Acta **53**, 6835 (2008).
- 34) National Astronomical Observatory of Japan, *Chronological Scientific Tables* (Maruzen Co., Ltd., Tokyo, 2002) p. 380, 389, 518 [in Japanese].

Figure Captions

Fig. 1. (Color online) Schematic illustration of the overall experimental setup and a method for forming a BLM. (a) The Si chip was sandwiched between the Teflon chambers; 2 M KCl and 5 mM HEPES mixed buffer solution was poured in both wells. EIS was conducted with a chemical potentiostat in a Faraday cage. (b) (left) The aperture-suspended BLM with the Si chip, (middle) a cross-sectional view, (right) side view of the frustum area. (c) Free-standing BLMs were formed by using the folding method.¹⁾

Fig. 2. (Color online) (a) Equivalent circuit model I proposed in previous research.¹⁷⁾ (b) Equivalent circuit model II including $R_{EDL}C_{EDL}$ parallel circuits for the EDL effects on both sides of BLM, and equivalent circuit model III including the $R_{EDL}Q_{EDL}$ parallel circuits proposed in this study.

Fig. 3. (Color online) (a) The results of EIS measurement (plots) and fitting curves of the circuit model I-II (dashed black lines) and III (solid color lines). (b) The relative fitting errors were calculated with the measured values as true values.

Fig. 4. Capacitance of electrical double layer calculated by Gouy-Chapman's theory²⁹⁻³⁰⁾ and Kornyshev's theory³²⁾ as a function of a dielectric constant. (a) The Gouy-Chapman's theoretical curve was calculated by using these values: temperature $T = 293$ K, bulk concentration $n_0 = 2$ M. (b) Kornyshev's theoretical curve calculated by using the same values of the Gouy-Chapman's theoretical curve. The additional parameter of $n_{\max} = 4.58$ M is the maximal possible local concentration of ions. It was calculated by using solubility, atomic weigh of KCl, and water density at 293 K.³⁴⁾

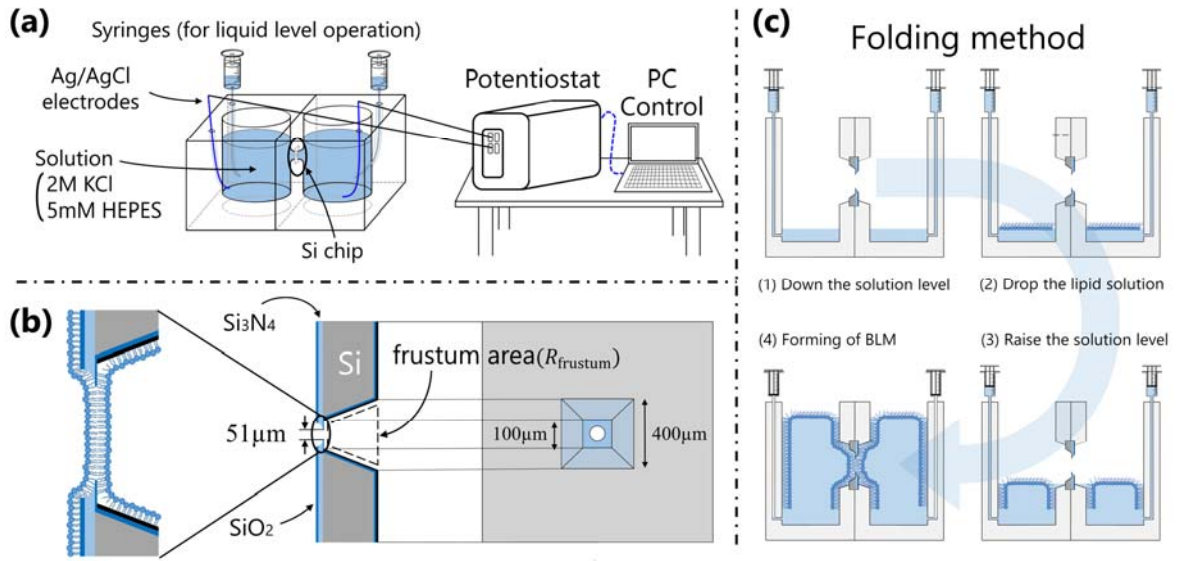


Fig. 1. (Color online)

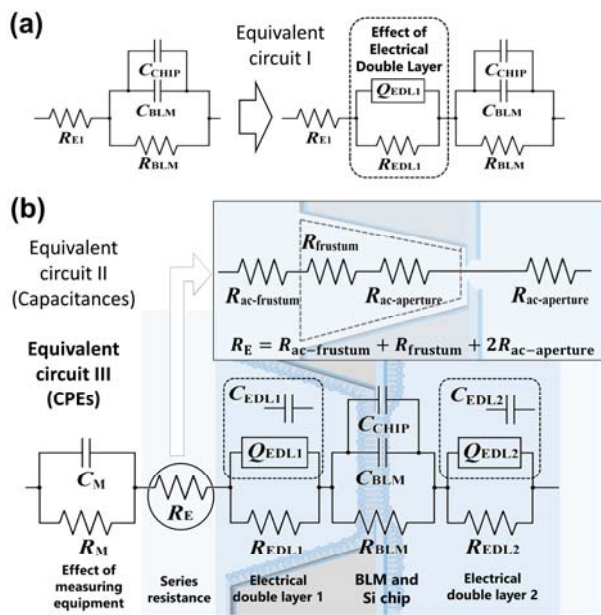


Fig. 2. (Color online)

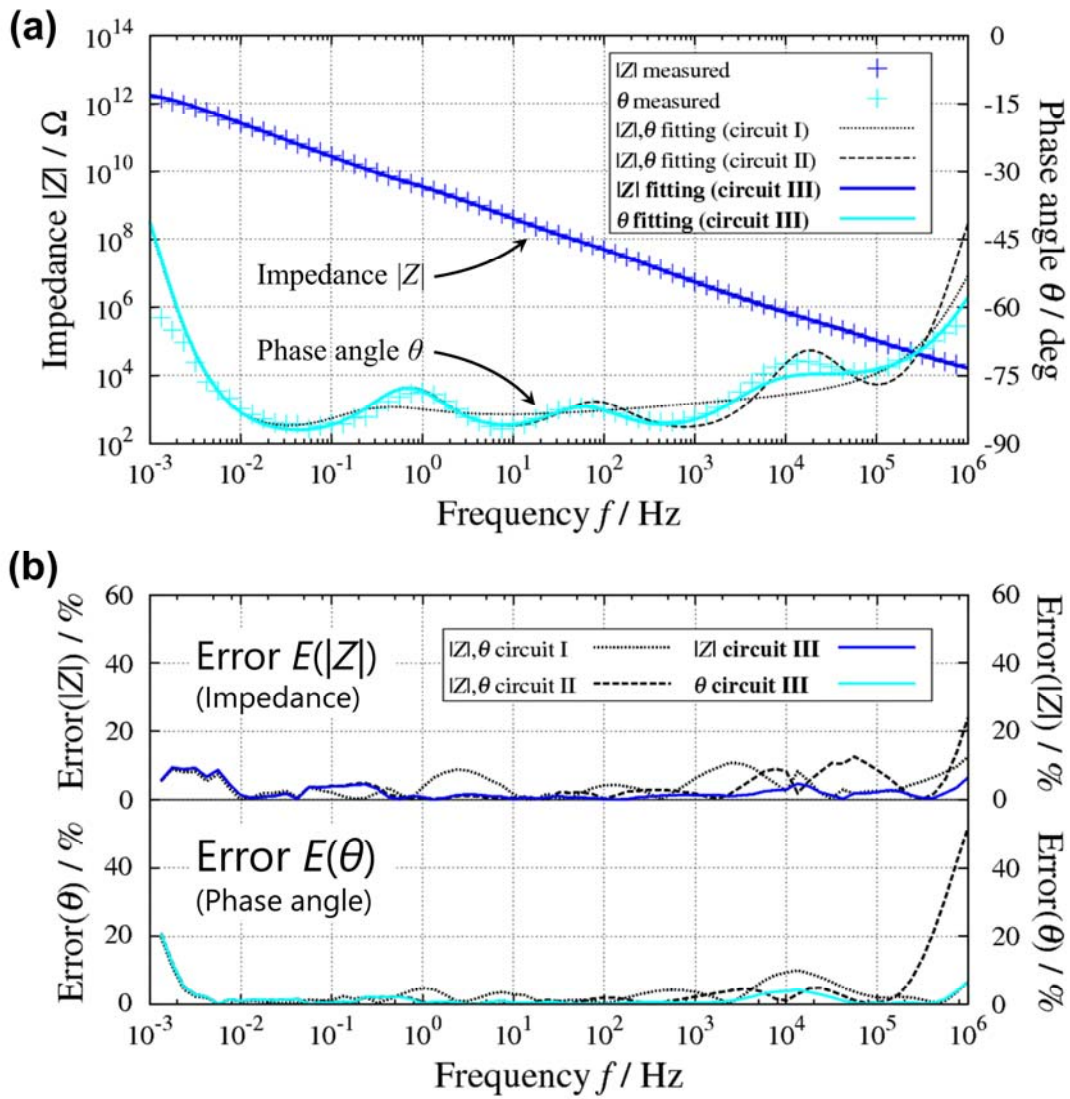


Fig. 3. (Color online)

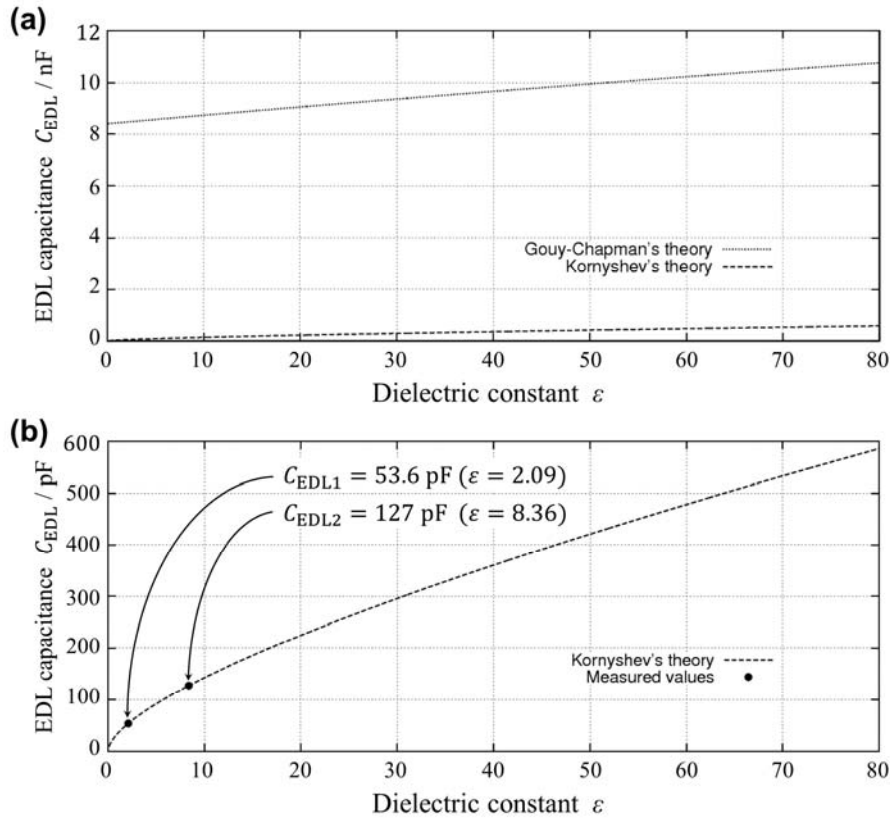


Fig. 4.

Table I. Parameters extracted from fitting results of equivalent circuit model I, II and III.

Circuit type	BLM and chip		Electrical double layer I			
	$R_{BLM}/T\Omega$	$C_{BLM} + C_{CH}/pF$	$R_{EDL1}/k\Omega$	Q_{EDL1}/pFs^{q-1}	C_{EDL1}/pF	α_1
Circuit I	2.37	60.3	3160000	225	209	0.82
Circuit II	2.33	59.5	222	-	29.2	-
Circuit III	2.34	59.4	456	632	53.6	0.77

Circuit type	Electrical double layer II				Other elements		
	$R_{EDL2}/M\Omega$	Q_{EDL2}/pFs^{q-1}	C_{EDL2}/pF	α_2	$R_M/G\Omega$	C_M/pF	$R_E/k\Omega$
Circuit I	-	-	-	-	-	-	6.95
Circuit II	16.1	-	106	-	1.63	111	12.3
Circuit III	18.5	132	127	0.99	1.65	113	5.32